Robotica (2016) volume 34, pp. 1383–1402. © Cambridge University Press 2015
doi:10.1017/S0263574714002355

Inverse and forward dynamics of N-3RPS manipulator with lockable joints

Ali Taherifar†, Hassan Salarieh†*, Aria Alasty† and Mohammad Honarvar‡

†*Department of Mechanical Engineering, Sharif University of Technology, Tehran, Iran*
‡*Department of Mechanical Engineering, UBC University, Canada*

(Accepted August 12, 2014. First published online: January 2, 2015)

SUMMARY
The N-3 Revolute-Prismatic-Spherical (N-3RPS) manipulator is a kind of serial–parallel manipulator and has higher stiffness and accuracy compared with serial mechanisms, and a larger workspace compared with parallel mechanisms. The locking mechanism in each joint allows the manipulator to be controlled by only three wires. Modeling the dynamics of this manipulator presents an inherent complexity due to its closed-loop structure and kinematic constraints. In the first part of this paper, the inverse kinematics of the manipulator, which consists of position, velocity, and acceleration, is studied. In the second part, the inverse and forward dynamics of the manipulator is formulated based on the principle of virtual work and link Jacobian matrices. Finally, the numerical example is presented for some trajectories.

KEYWORDS: Redundant manipulator; Inverse dynamics; Lockable joints; Virtual work.

Abbreviations and Nomenclature

a_i	= Position vector of the revolute joint (A_i)
b_i	= Position vector of the ball joint (B_i)
CAD	= Computer-Aided Design
d_i	= Length of limbs
${}^{Ai}F_{1i}$, ${}^{Ai}F_{2i}$	= Resultant load on cylinder and piston
f_e, n_e	= External force and moment on upper platform
F_p	= Resultant load on upper platform
HRM	= Hybrid Redundant Manipulator
${}^{Ai}I_{1i}$, ${}^{Ai}I_{2i}$	= Moment of inertia of cylinder and piston of the ith limb in its frame
${}^{0}I_p$	= Moment of inertia of upper platform
${}^{Ai}J_{1i}$, ${}^{Ai}J_{2i}$	= Link Jacobian matrices
J_p	= Manipulator Jacobian matrix
m_p	= Mass of upper platform
p	= Position vector of point P
q	= Vector of limb length
R_0^{Ai}	= $\left[{}^{x}R_0^{Ai}\ {}^{y}R_0^{Ai}\ {}^{z}R_0^{Ai}\right]^T$ rotation matrix from the base frame to the limb frame
R_1^0	= rotation matrix from frame 1 to the base frame
RPS	= Revolute-Prismatic-Spherical
r_{up}	= Vector points from the center of the upper platform of the nth link to the end-effector
r_{down}	= Position vector of the lower platform of the nth link
r_{CG}	= Position vector of the center of mass of moving parts
s_i	= $\left[s_{ix}\ s_{iy}\ s_{iz}\right]^T$ unit vector along the limbs

* Corresponding author. E-mail: salarieh@sharif.edu

SPM = Serial–Parallel Manipulator
SPR = Spherical-Prismatic-Revolute
SPS = Spherical-Prismatic-Spherical
τ = Input force of actuator
u, v, w, = First, second, and third column of R_1^0 rotation matrix
v_p = Linear velocity of the center of mass of upper platform
v_{bi} = $\left[v_{bi}^x \; v_{bi}^y \; v_{bi}^z \right]^T$ velocity of the ball joint (B_i)
${}^{Ai}\omega_i$ = Angular velocity of the ith limb in its frame
ω_p = Angular velocity of upper platform
$\dot{x}_p$ = $\left[v_p \; \omega_p \right]^T$ velocity of the end-effector

1. Introduction

Kinematically redundant manipulators have more degrees of freedom (DOF) than required for determining the position and orientation of an end-effector.[1] Due to their high flexibility, they have a great potential to work in fully constrained, complex, and hazardous environments such as nuclear reactors and space stations.[2] They can also be used for surgery, exploration, and rescue operations.

This section is divided into two parts. The first part focuses on the researches that attempt to mechanically resolve the redundancy of hyper-redundant manipulators. The second part reviews the studies that address the kinematic and dynamic analysis of SPMs.

In the past two decades, many redundant manipulators with various structures and different actuation types have been proposed. Ning and Worgotte[3] have built a new 3D modular HRM. All the joints of this manipulator are passive, state-controllable, and share common input introduced by wire-driven control. Meghdari *et al*.[4,5] proposed a re-configurable manipulator with two arms. The arms normally operate redundantly, but when needed, they can lock into each other at certain joints to achieve a higher stiffness while losing some degrees of freedom.

Recently, new type of redundant manipulator in the sense of structure has been introduced, which is called SPM. SPMs have several modules with parallel structure that are connected serially. SPMs have the advantages of both serial manipulators (SMs) and parallel manipulators (PMs). This kind of manipulator has higher stiffness and accuracy compared with SM, and a larger workspace compared with PM.[6] Hu *et al.*[6] presented a novel 3RPS–3SPR SPM and solved inverse kinematics and active forces. The workspace of this SPM is constructed using the CAD variation geometry approach. Gallardo *et al.*[7–9] addressed the kinematic analysis, including position, velocity, and acceleration, of a modular spatial hyper-redundant manipulator built with a variable number of serially connected mechanical modules. They used the Screw theory and the principle of virtual work. Tanev[10] solved the forward and inverse position problem of a hybrid 2(SPS) manipulator. This paper addresses the kinematic and dynamic analysis of an SPM presented in Honarvar.[11]

In 2009, a novel tendon-actuated hyper-redundant manipulator was introduced by Honarvar.[11]. Figure 1(a) shows the four-link manipulator fabricated at Sharif University of Technology. The novelty of this tendon-actuated manipulator is the use of a locking mechanism at its joints, which makes it possible to be controlled with only three cables. Therefore, by releasing and locking the links in an arbitrary sequence and by stretching the cables, the configuration of the manipulator will change. This manipulator has serial–parallel structure and each link consists of a 3RPS parallel mechanism. The links are arranged serially to construct the manipulator. It should be noted that the term "serial–parallel manipulator" usually refers to a robot obtained by serially connecting *two* parallel manipulators. Detailed description of the manipulator is presented in Section 2. This paper addresses the systematic analysis of kinematics and dynamics of the manipulator introduced by Honarvar.[11] Dynamics modeling is essential for design specifications and advanced control of robots.[12] The dynamics of this manipulator presents an inherent complexity due to its closed-loop structure and kinematic constraints.

Several approaches have been proposed for the analysis of dynamics of the 3-RPS mechanism, including the Newton–Euler formulation,[12] the Lagrangian formulation,[13] and the principle of virtual work.[13–17] Other approaches have also been suggested.[18] A comparison study of inverse dynamics of manipulators with closed-loop geometry can be found in the work of Lin and Song.[19] Khalil solved kinematics and dynamics of 3-RPS mechanism by customized Newton–Euler algorithm.[15] In

https://doi.org/10.1017/S0263574714002355 Published online by Cambridge University Press

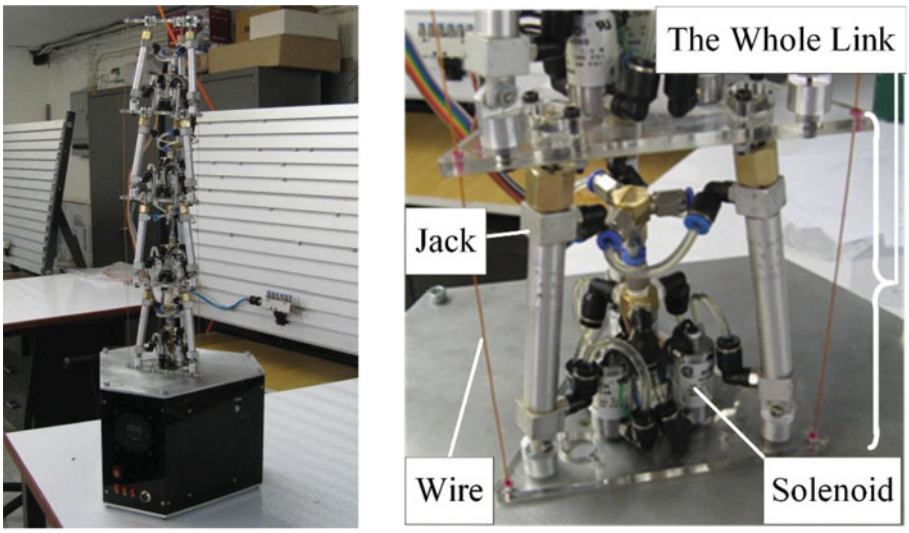

Fig. 1. (a) A 4-link manipulator with lockable joints designed and fabricated in Sharif University of Technology. (b) A link of a fabricated manipulator.

addition, Song studied a force-compensating device based on this mechanism.[19] Khalil and Ibrahim[12] presented a general method to calculate the inverse and direct model of dynamics of parallel robots. The models were expressed in a closed form by a single equation. Staicu[20] presented compact matrix dynamics equations, and the power requirement of each actuator in two different actuation schemes. Li *et al*.[21] formulated a semi-analytic stiffness model of 3RPS modules by taking into account the component compliances associated with actuations and constraints. Staicu[22,23] developed a recursive matrix approach in kinematics and dynamics modeling of parallel mechanisms. Here a full dynamic analysis of the 3RPS mechanism by the principle of virtual work and link Jacobian matrices is introduced. The analysis includes mass and inertia of piston and cylinder of each limb. Some illustrative examples are also included.

In the next section a detailed description of the manipulator is presented. In Section 3, the inverse and forward dynamic analysis of the 3RPS manipulator is presented. In Section 4, the kinematic and dynamic analyses of N-3RPS with lockable joints are described. The numerical example is presented in Section 5. Finally, the paper is concluded in Section 6.

2. Manipulator Description

In order to have a deep understanding of manipulator, it is essential to have its extended description. Each link of the manipulator consists of three hydraulic jacks (these are also called limbs), which are arranged in a parallel configuration (3RPS). The lengths of these jacks are rather fixed (locked) or varying (unlocked) due to solenoids states. The solenoid valves are the main components of locking mechanism and are put in a hydraulic circuit as shown in Fig. 2. Once they are chosen to be unlocked, the length of jacks is controlled by wires.

The upper ports of jacks are connected to each other via tiny pipes. It means that the sum of oil flow above pistons and inside cylinders is constant. Similarly, lower ports are connected to each other, while three solenoid valves are put in the way to block oil flow at any desired time. In our application, all solenoid valves are opened or closed simultaneously. Although it is possible to open two solenoids, this is not considered in this paper.

Imagine the jacks to be in their equilibrium position and all solenoids are closed as shown in Fig. 2 (left). In this state, all jacks are locked. Now the solenoid valves are opened as shown in Fig. 2 (right) and the first and second jacks are moved d meters downwards. Consequently, the oil under the piston of the first and second jacks will flow to the third cylinder and result in the upward displacement of $2d$ meters in the third jack. In order to perform this scenario practically, the first and second wires

https://doi.org/10.1017/S0263574714002355 Published online by Cambridge University Press

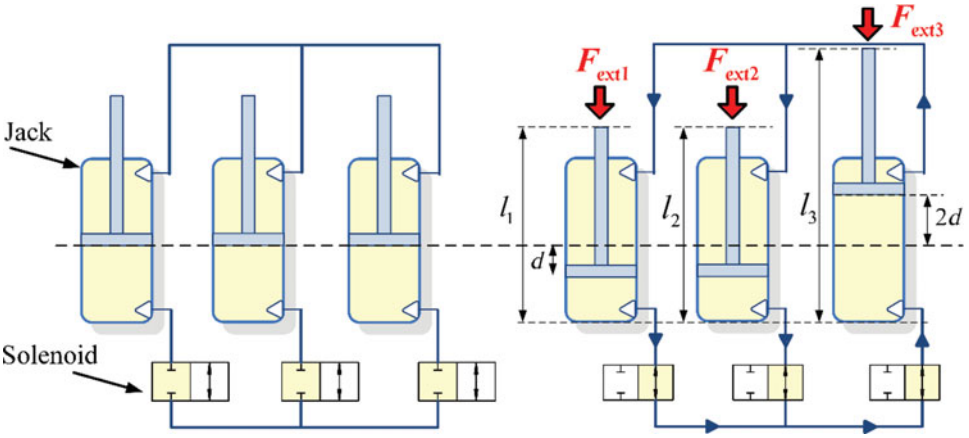

Fig. 2. The hydraulic circuit of locking system in each link.

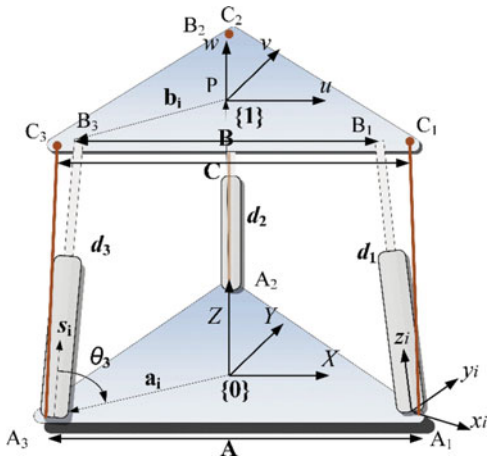

Fig. 3. Schematic of a manipulator with 3RPS mechanism. Cables are passed through C_i points.

are drawn and pushed to the corresponding jacks downwards and the third jack is force-controlled to keep the wire stretched.

Therefore, there is a constraint between jacks' length since the amount of oil on the top and the bottom of pistons is constant. The constraint equation is

$$d_1 + d_2 + d_3 = \text{const}, \tag{1}$$

where d_1, d_2, d_3 are the lengths of jacks. The 3RPS mechanism has 3 DOF (Fig. 3). The constraint of the locking mechanism reduces 1 DOF when all solenoid valves are open. Therefore, each link has 2 DOF.

The hydraulic circuit shown in Fig. 2 also imposes a constraint equation on external forces. The equation of motion of each leg can be written as

$$F_{\text{ext}} - F_{\text{pressure}} = m\ddot{d}_i, \quad i = 1, 2, 3, \tag{2}$$

where F_{pressure} is the force generated by the oil pressure and is equal to $P_1A_1 - P_2A_2$, where P_1, P_2 are the oil pressure on the bottom and the top of piston respectively and A_1, A_2 are the cross section areas of piston respectively. Now three equations expressed in (2) are summed as

$$F_{\text{ext1}} + F_{\text{ext2}} + F_{\text{ext3}} - 3F_{\text{pressure}} = m\underbrace{(\ddot{d}_1 + \ddot{d}_2 + \ddot{d}_3)}_{0}. \tag{3}$$

https://doi.org/10.1017/S0263574714002355 Published online by Cambridge University Press

Note that $\ddot{d}_1 + \ddot{d}_2 + \ddot{d}_3 = 0$ according to Eq. (1). Finally, we have

$$F_{\text{pressure}} = \frac{F_{\text{ext1}} + F_{\text{ext1}} + F_{\text{ext1}}}{3}. \tag{4}$$

Therefore, there is a constraint equation between the external forces applied on the jacks. This equation will be used in the inverse dynamic analysis.

Actuators are three cables that pass through joints all along the arm as shown in Fig. 1(b). The solenoid valves, jacks, and wires are shown clearly in this figure. The wire ends are knotted on most of the top points of manipulator. When a link is locked, the position and orientation of that link remain unchanged. In this paper, a parallel mechanism, and its corresponding locking system, is called a *link*. At any time, all links of a manipulator are locked except one. Whenever the cables are moved by winch and motors, the manipulator will tilt to its new position, while all locked joints move as a rigid body. It is worth mentioning that the hydraulic jacks are not actuated by hydraulic pump and servo valves but are actuated by wires indirectly. Using the lockable joints will decrease the number of motors and reduce the total weight and cost. An 8-DOF prototype has been designed and made in Sharif University of Technology for practical experiments (Fig. 1). The manipulator has inner-loop force control that keeps wires tension always positive.

Generally, parallel manipulators inherently have high stiffness and limited workspace. These have their industrial applications in spite of their limitations. In this paper, the effective mobility of a 3-RPS manipulator is increased by connecting 3-RPS mechanism serially. Shafahi has optimized and utilized the manipulator in 2011.[24] Although the structure of the manipulator is simplified by this novel idea, the path planning and control problem are complicated enormously. Taherifar *et al.*[25] studied the path planning of this manipulator using particle swarm optimization.

3. Kinematics of 3RPS Manipulator

The first step in the analysis of N-3RPS manipulator is the kinematic analysis of a single 3RPS mechanism. Figure 3 illustrates the 3RPS mechanism. A fixed coordinate frame (*XYZ*) is attached to the lower platform and a moving coordinate frame (*uvw*) is attached to the upper platform. The origin of (*uvw*) frame is located at the point P, the center of volume of the upper platform. Here we focus on the inverse kinematics of the mechanism since it is essential in dynamic analysis of the manipulator. In the 3RPS mechanism the orientation of the upper platform is related to the position of the platform by some constraint equations, which cause some difficulties in the dynamic analysis of the manipulator. In other words, the moving platform has simultaneously six mixed motions (three translations coupled with three relative concurrent rotations about its center), but the motion in general translation and orientation degrees of freedom is interconnected, as three of the six position variables represent three parasitic parameters given by some geometric constraint relations. The kinematics of the mechanism is analyzed using the link Jacobian concept similar to the one given inTsai.[14]

3.1. Inverse kinematics

By definition, the inverse kinematic analysis is the calculation of lengths of limbs when the position of the upper platform is known priorly. Here the x- and y-component of the position of upper platform are known and the z-component is constrained since Eq. (1) reduces the mechanism to 2 DOF. The first step in the inverse kinematic analysis of the 3RPS mechanism is the calculation of the orientation of the upper platform. The orientation is defined by the rotation matrix between upper and lower platforms. The positions of the end points of limbs (B_i) in a fixed coordinate frame are

$$\begin{aligned} B_1 &= p + b_1, \\ B_2 &= p + b_2, \\ B_3 &= p + b_3, \end{aligned} \tag{5}$$

$$b_1 \quad = R_1^0 \begin{bmatrix} \frac{B}{2} & \frac{-B}{2\sqrt{3}} & 0 \end{bmatrix}^T,$$

https://doi.org/10.1017/S0263574714002355 Published online by Cambridge University Press

$$b_2 = R_1^0 \begin{bmatrix} 0 & \frac{B}{\sqrt{3}} & 0 \end{bmatrix}^T,$$
$$b_3 = R_1^0 \begin{bmatrix} \frac{-B}{2} & \frac{-B}{2\sqrt{3}} & 0 \end{bmatrix}^T,$$
$$R_1^0 = \begin{bmatrix} u_x & v_x & w_x \\ u_y & v_y & w_y \\ u_z & v_z & w_z \end{bmatrix}, \tag{6}$$

where p is the position vector of point P and R_1^0 is the rotation matrix from the moving coordinate frame to the fixed one. B is the side of the upper triangle as shown in Fig. 3. The positions of points B_i, B_2, B_3 can be written as

$$B_1 = \begin{bmatrix} p_x + \frac{1}{2}Bu_x - \frac{1}{2\sqrt{3}}Bv_x \\ p_y + \frac{1}{2}Bu_y - \frac{1}{2\sqrt{3}}Bv_y \\ p_z + \frac{1}{2}Bu_z - \frac{1}{2\sqrt{3}}Bv_z \end{bmatrix}, \; B_2 = \begin{bmatrix} p_x + \frac{Bv_x}{\sqrt{3}} \\ p_y + \frac{Bv_y}{\sqrt{3}} \\ p_z + \frac{Bv_z}{\sqrt{3}} \end{bmatrix}, B_3 = \begin{bmatrix} p_x - \frac{1}{2}Bu_x - \frac{1}{2\sqrt{3}}Bv_x \\ p_y - \frac{1}{2}Bu_y - \frac{1}{2\sqrt{3}}Bv_y \\ p_z - \frac{1}{2}Bu_z - \frac{1}{2\sqrt{3}}Bv_z \end{bmatrix}. \tag{7}$$

Since the revolute joints do not let any motion out of the revolute axis, the following constraints must be included in analysis:

$$B_{1x} = -\sqrt{3}B_{1y},$$
$$B_{2x} = 0,$$
$$B_{3x} = \sqrt{3}B_{3y}. \tag{8}$$

Substituting Eq. (7) into (8) yields

$$P_x + \frac{Bv_x}{\sqrt{3}} = 0,$$
$$v_x = u_y,$$
$$P_y = \frac{B}{2\sqrt{3}}(v_y - u_x), \tag{9}$$

which represent just three constraint relations giving three parasitic parameters. The definition of the rotation matrix will impose the following equations:

$$u_x^2 + u_y^2 + u_z^2 = 1,$$
$$v_x^2 + v_y^2 + v_z^2 = 1,$$
$$w_x^2 + w_y^2 + w_z^2 = 1,$$
$$u_x v_x + u_y v_y + u_z v_z = 0,$$
$$u_x w_x + u_y w_y + u_z w_z = 0,$$
$$v_x w_x + v_y w_y + v_z w_z = 0. \tag{10}$$

The orientation of the moving platform is completely described by the general rotation matrix R_1^0. The Euler representation can be adopted to describe the absolute moving platform posture, which comprises three successive relative rotations, namely: the first rotation of angle α_z around the *w'*-axis, followed by the second rotation of angle α_y around the rotated *v"*-axis, and finally followed by the third rotation of angle α_x around the *u*-axis of the moving frame (*uvw*) attached to the moving platform. With respect to the fixed global coordinate system (*XYZ*), the general rotation matrix can be expressed by a multiplication of three known basic rotation matrices as $R_1^0 = R(\omega', \alpha_z)R(v'', \alpha_y)R(u, \alpha_x)$. Referring

https://doi.org/10.1017/S0263574714002355 Published online by Cambridge University Press

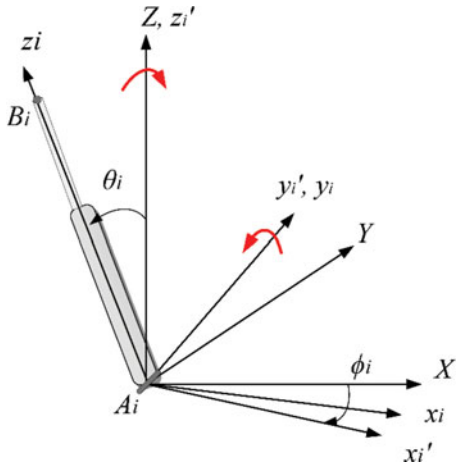

Fig. 4. Euler angles of a limb.

to Fig. 3, the kinematic loop can be written as

$$\begin{aligned} a_i + d_i s_i &= p + b_i, \\ s_i &= (p + b_i - a_i)/d_i, \\ d_i &= \| p + b_i - a_i \|, \end{aligned} \tag{11}$$

where s_i is the unit vector along the ith limb, and d_i is the length of the limb. Since each link has 2 DOF due to the constraint Eq. (1), the inputs of inverse kinematics are P_x, P_y. It must be noted that P_z is calculated by inverse kinematic equations. So the nonlinear Eqs. (1), (9), and (10) are solved together. The solution of these 12 equations will give the limbs' length (d_1, d_2), P_z, and nine elements of the rotation matrix (R_1^0).

Another coordinate frame $A_i(x_i, y_i, z_i)$ is attached to each limb as shown in Fig. 3. The z_i-axis points from A_i to B_i, and the y_i-axis coincides with the axis of revolute joint at A_i. If the base coordinate frame is rotated by ϕ_i about the z-axis, frame $A_i(x_i', y_i', z_i')$ is created as shown in Fig. 4. Then this frame is rotated by θ_i about y_i' to result in $A_i(x_i, y_i, z_i)$ coordinate frame, which is called the ith limb frame. The rotation matrix from the $A_i(x_i, y_i, z_i)$ frame to the base frame (XYZ) is

$$R_{Ai}^0 = \begin{bmatrix} c\phi_i c\theta_i & -s\phi_i & c\phi_i s\theta_i \\ s\phi_i c\theta_i & c\phi_i & s\phi_i s\theta_i \\ -s\theta_i & 0 & c\theta_i \end{bmatrix}. \tag{12}$$

The unit vector along the limbs (s_i) in the base frame is

$$s_i = \begin{bmatrix} c\phi_i s\theta_i \\ s\phi_i s\theta_i \\ c\theta_i \end{bmatrix}, \tag{13}$$

where ϕ_i is a constant and θ_i can be obtained by the following equation in radians,

$$\begin{aligned} \theta_i &= \tan^{-1}(\sqrt{s_{ix}^2 + s_{iy}^2}/s_{iz}) \ , (0 \le \theta \le \pi), \\ \phi &= \begin{bmatrix} -\pi/6 & \pi/2 & 7\pi/6 \end{bmatrix}. \end{aligned} \tag{14}$$

https://doi.org/10.1017/S0263574714002355 Published online by Cambridge University Press

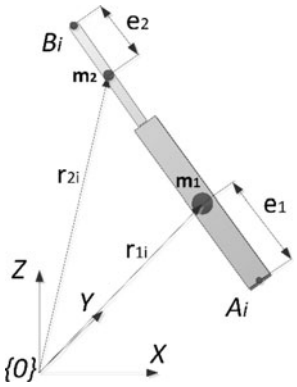

Fig. 5. Geometrical parameter of a limb.

Figure 5 shows limb's geometrical parameter. The following relations formulate the position of mass center of piston and cylinder,

$$\begin{aligned} r_{1i} &= a_i + e_1 s_i, \\ r_{2i} &= a_i + (d_i - e_2) s_i. \end{aligned} \tag{15}$$

The derivative of the right-hand side of Eq. (11) is taken to obtain the velocity of B_i,

$$v_{bi} = v_p + \omega_p \times b_i = v_p + s(b_i)\omega_p, \tag{16}$$

where $s(.)$ is the skew-symmetric matrix defined by

$$s(m) = \begin{bmatrix} 0 & m_z & -m_y \\ -m_z & 0 & m_x \\ m_y & -m_x & 0 \end{bmatrix}. \tag{17}$$

The velocity of point B_i is transformed to the ith limb frame by multiplying the rotation matrix

$${}^{Ai}v_{bi} = R_0^{Ai} v_{bi}. \tag{18}$$

The rotation matrix R_0^{Ai} is the transpose of R_{Ai}^0 as defined in Eq. (12). For further formulation, it is better to parameterize the rotation matrix as $R_0^{Ai} = [\,{}^x R_0^{Ai} \quad {}^y R_0^{Ai} \quad {}^z R_0^{Ai}\,]^T$, where ${}^x R_0^{Ai}$ is the first row of R_0^{Ai} and so on. Once again the constraint equation imposed by revolute joints must be considered. Since the point B_i does not have velocity in the revolute axis direction, we have:

$${}^{Ai}v_{bi}^y = 0. \tag{19}$$

Substituting Eqs. (16) to (18), the constraint Eq. (19) can be written as

$$\begin{aligned} \underbrace{{}^y R_0^{Ai}}_{c_2} v_p + \underbrace{{}^y R_0^{Ai} s(b_i)}_{-c_1} \omega_p &= 0, \\ \omega_p = c_1^{-1} c_2 v_p &= c v_p. \end{aligned} \tag{20}$$

Equation (20) formulates a constraint relation between the linear and angular velocities of upper platform, where c, c_1, and c_2 are 3×3 matrices. The linear velocity of ith piston is $\dot{d}_i = {}^{Ai}v_{bi}^z$. The derivative of Eq. (1) constrains the linear speed of limbs ($\dot{d}_1 + \dot{d}_2 + \dot{d}_3 = 0$). So one can use the following equation for the rate of every limb's longitudinal motion:

$$\dot{d}_i = {}^{Ai}v_{bi}^z = {}^z R_0^{Ai} v_p + {}^z R_0^{Ai} s(b_i) c v_p. \tag{21}$$

https://doi.org/10.1017/S0263574714002355 Published online by Cambridge University Press

Equations (1) and (21) are solved together to obtain $\dot{d}_1, \dot{d}_2$, and v_{pz}.

On the other hand, the derivative of the left-hand side of Eq. (11) is taken and expressed in the ith limb coordinate frame,

$$^{Ai}v_{bi} = d_i\,{}^{Ai}\omega_i \times {}^{Ai}s_i + \dot{d}_i\,{}^{Ai}s_i, \tag{22}$$

where $^{Ai}s_i = R_0^{Ai}s_i$. Considering the fact that the jack does not rotate about its longitudinal axis ($\omega_i^T s_i = 0$) and cross-multiplying both side of Eq. (22) by $^{Ai}s_i$ yields the angular velocity of the limb

$$^{Ai}\omega_i = \frac{1}{d_i}(^{Ai}s_i \times {}^{Ai}v_{bi}), \tag{23}$$

where $^{Ai}s_i = [\,0 \quad 0 \quad 1\,]^T$. Taking the derivative of Eq. (15) and performing some simplification,

$$\begin{aligned} v_{1i} &= e_1\,{}^{Ai}\omega_i \times {}^{Ai}s_i, \\ v_{2i} &= (d_i - e_2)^{Ai}\omega_i \times {}^{Ai}s_i + \dot{d}_i\,{}^{Ai}s_i. \end{aligned} \tag{24}$$

In order to perform acceleration analysis, the derivative of Eq. (20) is taken to derive the relation between the linear and angular accelerations of upper platform,

$$\begin{aligned} c_1\dot{\omega}_p + \dot{c}_1\omega_p &= c_2\dot{v}_p, \\ \dot{\omega}_p &= c\dot{v}_p - c_1^{-1}\dot{c}_1 c v_p, \\ \dot{c}_1 &= {}^{y}R_0^{Ai} \times (s(b_i)\omega_p). \end{aligned} \tag{25}$$

The acceleration of point B_i is obtained by taking the derivative of Eqs. (16) and (18),

$$\begin{aligned} \dot{v}_{bi} &= \dot{v}_p + \dot{\omega}_p \times b_i + \omega_p \times (\omega_p \times b_i), \\ {}^{Ai}\dot{v}_{bi} &= R_0^{Ai}\dot{v}_{bi}, \end{aligned} \tag{26}$$

where $^{Ai}\dot{v}_{bi}$ is the acceleration of B_i in the ith limb coordinate frame. On the other hand, the linear acceleration of the piston and the angular acceleration of the jack can be determined from the derivative of Eq. (22) and considering that $\dot{\omega}_i^z = 0$,

$$\begin{aligned} \ddot{d}_i &= {}^{Ai}\dot{v}_{bi}^T\,{}^{Ai}s_i + d_i\,{}^{Ai}\omega_i^2, \\ {}^{Ai}\dot{\omega}_i &= \frac{1}{d_i}\,{}^{Ai}s_i \times {}^{Ai}\dot{v}_{bi} - \frac{2\dot{d}_i}{d_i}\,{}^{Ai}\omega_i. \end{aligned} \tag{27}$$

The derivative of Eq. (1) constrains the linear acceleration of limbs ($\ddot{d}_1 + \ddot{d}_2 + \ddot{d}_3 = 0$). So Eqs. (1), (26), and (27) are solved together to find $\ddot{d}_1, \ddot{d}_2$, and $\dot{v}_{pz}$.

Similarly, the accelerations of the center of mass of piston and cylinder are calculated by the following formulation:

$$\begin{aligned} {}^{Ai}\dot{v}_{1i} &= e_1\,{}^{Ai}\dot{\omega}_i \times {}^{Ai}s_i + e_1\,{}^{Ai}\omega_i \times (^{Ai}\omega_i \times {}^{Ai}s_i), \\ {}^{Ai}\dot{v}_{2i} &= \ddot{d}_i\,{}^{Ai}s_i + (d_i - e_2)^{Ai}\dot{\omega}_i \times {}^{Ai}s_i + (d_i - e_2)^{Ai}\omega_i \times (^{Ai}\omega_i \times {}^{Ai}s_i) + 2\dot{d}_i\,{}^{Ai}\omega_i \times {}^{Ai}s_i. \end{aligned} \tag{28}$$

3.2. Jacobian matrices

The link Jacobian is introduced to simplify the derivation of equation of motion of manipulator. Equation (16) can be written in the matrix form as

$$v_{bi} = J_{bi}\dot{x}_p,$$

https://doi.org/10.1017/S0263574714002355 Published online by Cambridge University Press

$$J_{bi} = \begin{bmatrix} 1 & 0 & 0 & 0 & b_i^z & -b_i^y \\ 0 & 1 & 0 & -b_i^z & 0 & -b_i^x \\ 0 & 0 & 1 & -b_i^y & -b_i^x & 0 \end{bmatrix}, \tag{29}$$

where $\dot{x}_p = [\, v_p \quad \omega_p \,]^T = [\, v_p \quad cv_p \,]^T$. Substituting Eq. (29) in Eq. (18) yields

$$^{Ai}v_{bi} = {}^{Ai}J_{bi}\dot{x}_p, \tag{30}$$

where $^{Ai}J_{bi} = R_0^{Ai}J_{bi}$. Since the linear (longitudinal) velocity of the piston is $\dot{d}_i = {}^{Ai}v_{bi}^z$ (the third row of $^{Ai}v_{bi}$), we have $\dot{d}_i = {}^{Ai}J_{bi}^z\dot{x}_p$, so

$$\begin{aligned} \dot{q} &= J_p\dot{x}_p, \\ J_p &= \begin{bmatrix} ^{A1}J_{b1}^z \\ ^{A2}J_{b2}^z \\ ^{A3}J_{b3}^z \end{bmatrix}, \end{aligned} \tag{31}$$

where $\dot{q} = [\, \dot{d}_1 \quad \dot{d}_2 \quad \dot{d}_3 \,]^T$, and J_p is known as the *manipulator Jacobian matrix*. Similarly, the velocity of point C_i, as shown on Fig. 3 (the cable passes through this point), can be written as

$$\begin{aligned} v_{ci} &= J_{ci}\dot{x}_p, \\ J_{ci} &= \begin{bmatrix} 1 & 0 & 0 & c_i^z & -c_i^y & \\ 0 & 1 & 0 & -c_i^z & 0 & -c_i^x \\ 0 & 0 & 1 & -c_i^y & -c_i^x & 0 \end{bmatrix}. \end{aligned} \tag{32}$$

Similarly, transforming the velocity of point C_i to a new frame and sorting the third row of velocity in the matrix form will result in

$$\begin{aligned} \dot{q}_t &= J_{pt}\dot{x}_p, \\ J_{pt} &= \begin{bmatrix} ^{A1}J_{c1}^z \\ ^{A2}J_{c2}^z \\ ^{A3}J_{c3}^z \end{bmatrix}, \end{aligned} \tag{33}$$

where J_{pt} is known as the *cable Jacobian matrix*. Similarly, combining Eqs. (23) and (24), writing the linear and angular velocity of piston and cylinder, we have

$$\begin{aligned} ^{Ai}\dot{x}_{1i} &= {}^{Ai}J_{1i}\dot{x}_p, \\ ^{Ai}\dot{x}_{2i} &= {}^{Ai}J_{2i}\dot{x}_p, \\ ^{Ai}J_{1i} &= \frac{1}{d_i}\begin{bmatrix} e_1{}^{Ai}J_{bi}^x \\ e_1{}^{Ai}J_{bi}^y \\ 0_{1\times 6} \\ -{}^{Ai}J_{bi}^y \\ {}^{Ai}J_{bi}^x \\ 0_{1\times 6} \end{bmatrix}, {}^{Ai}J_{2i} = \frac{1}{d_i}\begin{bmatrix} (d_i - e_2)^{Ai}J_{bi}^x \\ (d_i - e_2)^{Ai}J_{bi}^y \\ d_i{}^{Ai}J_{bi}^z \\ -{}^{Ai}J_{bi}^y \\ {}^{Ai}J_{bi}^x \\ 0_{1\times 6} \end{bmatrix}, \end{aligned} \tag{34}$$

where $^{Ai}J_{1i}$ and $^{Ai}J_{2i}$ are called the *link Jacobian matrices*.

https://doi.org/10.1017/S0263574714002355 Published online by Cambridge University Press

4. Dynamics of 3RPS Manipulator

The inverse dynamics modeling is important for the high performance control algorithms of robots, and the direct dynamics model is required for the simulation.[14]. In the next part, the inverse dynamics is formulated.

4.1. Inverse dynamics

In the inverse dynamics problem, the desired trajectory of upper platform is given and the required forces of linear actuators are to be determined. The principle of virtual work is used to drive the equation of motion and the required forces. The angular velocity of upper platform is related to linear velocity by Eq. (24).

When the external force and torque on the center of volume of upper platform are denoted by f_e and n_e respectively, the resultant load, including the inertial forces on the upper platform will be

$$F_p = \begin{bmatrix} f_p \\ n_p \end{bmatrix} = \begin{bmatrix} f_e + m_p g - m_p \dot{v}_p \\ n_e - {}^0 I_p \dot{\omega}_p - \omega_p \times ({}^0 I_p \omega_p) \end{bmatrix}, \tag{35}$$

where ${}^0 I_p$ is the moment of inertia of upper platform in the fixed coordinate frame and m_p is the mass of the aforementioned platform. Similarly, the resultant load on the cylinder and piston of the ith limb in its frame can be written as

$$\begin{aligned} {}^{Ai}F_{1i} &= \begin{bmatrix} f_{1i} \\ n_{1i} \end{bmatrix} = \begin{bmatrix} m_{1i} R_0^{Ai} g - m_{1i}\, {}^{Ai}\dot{v}_{1i} \\ -{}^{Ai} I_{1i} \dot{\omega}_i - {}^{Ai}\omega_i \times ({}^{Ai} I_{1i}\, {}^{Ai}\omega_i) \end{bmatrix}, \\ {}^{Ai}F_{1i} &= \begin{bmatrix} f_{2i} \\ n_{2i} \end{bmatrix} = \begin{bmatrix} m_{2i} R_0^{Ai} g - m_{2i}\, {}^{Ai}\dot{v}_{2i} \\ -{}^{Ai} I_{2i} \dot{\omega}_i - {}^{Ai}\omega_i \times ({}^{Ai} I_{2i}\, {}^{Ai}\omega_i) \end{bmatrix}, \end{aligned} \tag{36}$$

where ${}^{Ai}I_{1i}$ and ${}^{Ai}I_{2i}$ are the moment of inertia of cylinder and piston of the ith limb in the attached coordinate frame respectively. Here m_{1i} and m_{2i} are respectively the mass of cylinder and piston of the ith limb.

By the principle of virtual work, the equation of motion can be stated as

$$\delta q_t^T F_t + \delta q^T \tau + \delta x_p^T F_p + \sum_{i=1}^{6} ({}^{Ai}\delta \dot{x}_{1i}\, {}^{Ai}F_{1i} + {}^{Ai}\delta \dot{x}_{2i}\, {}^{Ai}F_{2i}) = 0 \oplus, \tag{37}$$

where F_t is the cable tension and τ is the limb force. Considering the Jacobian relations formulated in Eqs. (31), (33), and (34), one have $\delta q = J_p \delta x_p$, $\delta q_t = J_{pt} \delta x_p$, ${}^{Ai}\delta x_{1i} = {}^{Ai}J_{1i} \delta x_p$, and ${}^{Ai}\delta x_{2i} = {}^{Ai}J_{2i} \delta x_p$. On the other hand, the variation of position and orientation can be expressed as $\delta x_p = [\, \delta p \quad c\delta p \,]^T$. Consequently, Eq. (37) might be rewritten as

$$\begin{aligned} &\delta p^T \left[J_{pt}^T F_t + J_p^T \tau + F_p + \sum_{i=1}^{6} ({}^{Ai}J_{1i}\, {}^{Ai}F_{1i} + {}^{Ai}J_{2i}\, {}^{Ai}F_{2i}) \right]_{\text{row}=1,2,3} \\ &+ c\delta p^T \left[J_{pt}^T F_t + J_p^T \tau + F_p + \sum_{i=1}^{6} ({}^{Ai}J_{1i}\, {}^{Ai}F_{1i} + {}^{Ai}J_{2i}\, {}^{Ai}F_{2i}) \right]_{\text{row}=4,5,6} = 0. \end{aligned} \tag{38}$$

https://doi.org/10.1017/S0263574714002355 Published online by Cambridge University Press

Since δp^T is an independent variable, Eq. (38) takes its final form as

$$\overbrace{\left(\left[J_{pt}^T\right]_{\text{row}=1,2,3} + c\left[J_{pt}^T\right]_{\text{row}=4,5,6}\right)}^{E_1} F_t + \overbrace{\left(\left[J_p^T\right]_{\text{row}=1,2,3} + c\left[J_p^T\right]_{\text{row}=4,5,6}\right)}^{E_2} \tau + \underbrace{\left(\left[F_p + \sum_{i=1}^{6} ({}^{Ai}J_{1i}\,{}^{Ai}F_{1i} + {}^{Ai}J_{2i}\,{}^{Ai}F_{2i})\right]_{\text{row}=1,2,3} + c\left[F_p + \sum_{i=1}^{6} ({}^{Ai}J_{1i}\,{}^{Ai}F_{1i} + {}^{Ai}J_{2i}\,{}^{Ai}F_{2i})\right]_{\text{row}=4,5,6}\right)}_{E_3} = 0. \quad (39)$$

Equation (39) states the *equation of motion* of a cable-driven 3RPS manipulator in the presence of a constraint equation. In the inverse dynamics problem, the desired trajectory is given and the cables tension must be determined. The limbs force (τ) is determined according to Eq. (4). Equation (4) states that the limbs force is equal to the average of the external forces exerted on all limbs. Besides, the external forces on the limbs are due to the *tension forces* and *other dynamic terms*. Using Eq. (39), the limbs force is determined as follows:

$$\begin{aligned} &E_1 F_t + E_2 \tau + E_3 = 0, \\ &\tau = -M E_2^{-1}(E_1 F_t + E_3), \\ &M_{i,j} = \frac{1}{3} \quad \forall i, j, \end{aligned} \quad (40)$$

where M is a 3×3 square matrix with all elements equal to $1/3$, multiplying this matrix to a vector will give the average of the elements of that vector. So the cables tension can be determined by

$$\begin{aligned} &(E_1 - E_2 M E_2^{-1} E_1) F_t + (E_3 - E_2 M E_2^{-1} E_3) = 0, \\ &F_t = (E_1 - E_2 M E_2^{-1} E_1)^{-1}(E_3 - E_2 M E_2^{-1} E_3). \end{aligned} \quad (41)$$

Since the coefficient of F_t in Eq. (41) will be singular in numerical computation, there are infinite number of solutions for cables tension. The null space of the coefficient is [1 1 1], which means that the tension of all cables can be equally increased or decreased without deviating Eq. (39). So all cables can be initially stretched to a certain amount so that they do not have a negative tension during motion. In other words, since each link has 2 DOF and there are three wires to be controlled, there are infinite number of *positive* solutions for wires tension. For example, one can simply increase the average of tension and produce the same desired motion.

4.2. Forward dynamics

In the forward dynamics the input forces of actuators are given and the desired trajectory of the upper platform is to be determined. As described earlier, the 3RPS mechanism has 3 DOF, and the orientation of the manipulator is not an independent variable. So six state variables describing the position and linear velocity of the upper platform are defined as

$$Z = \begin{bmatrix} p \\ v_p \end{bmatrix}. \quad (42)$$

The goal of the forward dynamic analysis is to derive six ordinary differential equations. Equation (39) can be parameterized as

$$H_1 \dot{v}_p + H_2 = 0. \quad (43)$$

The state equations are as follows:

$$\dot{Z}_1 = Z_4,$$

https://doi.org/10.1017/S0263574714002355 Published online by Cambridge University Press

$$\begin{aligned}\dot{Z}_2 &= Z_5,\\ \dot{Z}_3 &= Z_6,\\ \begin{bmatrix}\dot{Z}_4\\ \dot{Z}_5\\ \dot{Z}_6\end{bmatrix} &= -H_1^{-1}H_2,\end{aligned} \tag{44}$$

where H_1 and H_2 are 3×3 matrices. Now the problem is to find H_1 and H_2 using Eqs. (35) and (36). The resultant loads on cylinder and piston are rewritten as

$$\begin{aligned}{}^{Ai}F_{1i} &= \begin{bmatrix} f_{1i-\text{coef}}\dot{v}_p + f_{1i-\text{cons}}\\ n_{1i-\text{coef}}\dot{v}_p + n_{1i-\text{cons}}\end{bmatrix} = {}^{Ai}F_{1i-\text{coef}}\dot{v}_p + {}^{Ai}F_{1i-\text{cons}},\\ {}^{Ai}F_{1i} &= \begin{bmatrix} f_{2i-\text{coef}}\dot{v}_p + f_{2i-\text{cons}}\\ n_{2i-\text{coef}}\dot{v}_p + n_{2i-\text{cons}}\end{bmatrix} = {}^{Ai}F_{2i-\text{coef}}\dot{v}_p + {}^{Ai}F_{2i-\text{cons}}.\end{aligned} \tag{45}$$

The coefficient of $\dot{v}_p$ in Eq. (35) might be extracted in the same way. It should be noted that $\dot{\omega}_p$ is a function of $\dot{v}_p$ and v_p according to Eq. (25). H_1 is the collection of $\dot{v}_p$ coefficients, while H_2 includes the terms that do not have $\dot{v}_p$ terms,

$$\begin{aligned}H_1 &= -m_p I_{3\times 3} - c\,{}^0I_p c + \left[\sum_{i=1}^{6}({}^{Ai}J_{1i}\,{}^{Ai}F_{1i-\text{coef}} + {}^{Ai}J_{2i}\,{}^{Ai}F_{2i-\text{coef}})\right]_{\text{row}=1,2,3}\\ &\quad + c\left[\sum_{i=1}^{6}({}^{Ai}J_{1i}\,{}^{Ai}F_{1i-\text{coef}} + {}^{Ai}J_{2i}\,{}^{Ai}F_{2i-\text{coef}})\right]_{\text{row}=4,5,6},\\ H_2 &= f_e + m_p g + c(n_e - {}^0I_p c_1^{-1}\dot{c}_1 c v_p) + \left[J_p^T\tau + \sum_{i=1}^{6}({}^{Ai}J_{1i}\,{}^{Ai}F_{1i-\text{cons}} + {}^{Ai}J_{2i}\,{}^{Ai}F_{2i-\text{cons}})\right]_{\text{row}=1,2,3}\\ &\quad + c\left[J_p^T\tau + \sum_{i=1}^{6}({}^{Ai}J_{1i}\,{}^{Ai}F_{1i-\text{cons}} + {}^{Ai}J_{2i}\,{}^{Ai}F_{2i-\text{cons}})\right]_{\text{row}=4,5,6} - \omega_p \times ({}^0I_p\omega_p).\end{aligned} \tag{46}$$

Finally, the trajectory of upper platform can be determined by solving the six ordinary differential equations in (44).

5. The N-3RPS Kinematics and Dynamics

The N-3RPS with lockable joint is an SPM described in Section 2. Figure 6 shows the schematic of the manipulator. Suppose that the *n*th link is unlocked and other links are locked as shown in Fig. 6. The coordinate frames are also shown in this figure. The first *n*–1 links are rigid and the vector ${}^0r_{\text{down}}$ is the position vector of lower platform of the *n*th link and is stated in the base coordinate frame. ${}^0r_{\text{up}}$ points from the center of the upper platform of the *n*th link to the end-effector and is also presented in the base coordinate frame. The kinematic and dynamic equations derived in Sections 3 and 4 can be used for the unlocked link with some modification.

Determination of the rotation matrix between the upper and lower platforms of unlocked link is the first step in the kinematic analysis. Second, the position vector of the upper platform must be calculated according to Eq. (11). Here the first and second steps are combined. The vector loop can be written as

$${}^0p = {}^0r_d - {}^0r_{\text{down}} - {}^0r_{\text{up}}, \tag{47}$$

https://doi.org/10.1017/S0263574714002355 Published online by Cambridge University Press

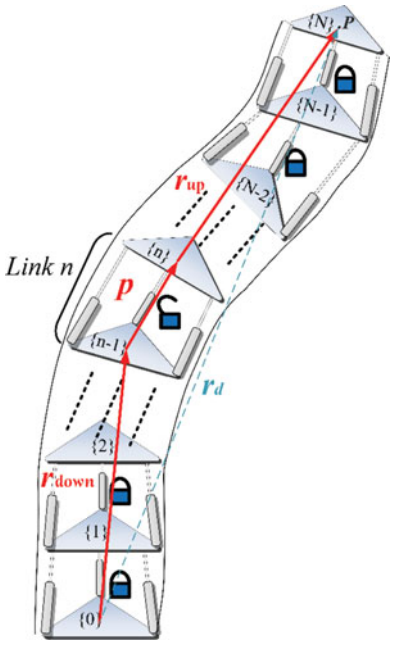

Fig. 6. Schematic of the cable-actuated hyper-redundant manipulator. The *n*th link is unlocked and others are locked. The coordinate frames are also shown.

where ${}^0r_d$ is the desired trajectory of end-effector. Equation (47) can be written in the form of

$$R_{n-1}^{0}\,{}^{n-1}p = {}^0r_d - {}^0r_{\text{down}} - R_{n-1}^{0}R_n^{n-1}\,{}^nr_{\text{up}}. \tag{48}$$

Note that ${}^{n-1}p$ can be extracted from Eq. (48) as

$${}^{n-1}p = R_0^{n-1}({}^0r_d - {}^0r_{\text{down}}) - \underbrace{R_n^{n-1}}_{\text{unknown}}\,{}^nr_{\text{up}}. \tag{49}$$

Since ${}^0r_d$ is given before and ${}^0r_{\text{down}}$ is known from the previous configuration of manipulator, the only unknown terms in the last equation are ${}^{n-1}p$ and R_n^{n-1}. In order to find R_n^{n-1} and ${}^{n-1}p$, Eqs. (1), (9), (10), and (49) should be solved together. The remaining formulations are the same except some mass and inertia properties.

As mentioned earlier, all links except the *n*th link are locked, and are consequently rigid. So the (*n*+1)th to *N*th links move together with the upper platform of the *n*th link. The mass and the moment of inertia of moving parts must include the mass and inertia of all elements above the platform,

$$\begin{aligned} m_{p-\text{new}} &= (N-n+1)m_p + 3(N-n)(m_1+m_2), \\ {}^nI_{p-\text{new}} &= \sum_{k=n}^{N} R_k^{nk}I_pR_n^k + 3\times\sum_{k=n+1}^{N} R_k^n({}^kI_{1i} + {}^kI_{2i})R_n^k, \end{aligned} \tag{50}$$

where ${}^kI_{1i}$ and ${}^kI_{1i}$ are the moment of inertia of cylinder and piston of the (*k*+1)th link in the *k*th coordinate frame respectively. In order to transform the moment of inertia to the *n*th frame, the rotation matrix must be multiplied from both sides. Finally, the resultant moment of inertia is transformed to the base frame by $R_n^{0n}I_{p-\text{new}}R_0^n$. Another point that should be noted is the moment produced by gravitational force. Since the center of mass of the moving part does not coincide with the center of volume, a moment is generated around the center of volume. The center of mass of the moving part

https://doi.org/10.1017/S0263574714002355 Published online by Cambridge University Press

Table I. The manipulator parameters.

Manipulator parameter	Value
A	0.1 m
B	0.08 m
m_p	126 gr
m_1	37 gr
m_2	4 gr
e_1	0.05 m
e_2	0.05 m
I_p	$\begin{bmatrix} 0.788 & 0 & 0 \\ 0 & 0.788 & 0 \\ 0 & 0 & 1.573 \end{bmatrix} \times 10^{-4}$ kg.m^2
I_1	$\begin{bmatrix} 2.284 & 0 & 0 \\ 0 & 2.284 & 0 \\ 0 & 0 & 0.112 \end{bmatrix} \times 10^{-5}$ kg.m^2
I_2	$\begin{bmatrix} 3.366 & 0 & 0 \\ 0 & 3.366 & 0 \\ 0 & 0 & 0.018 \end{bmatrix} \times 10^{-6}$ kg.m^2

is

$$r_{\mathrm{CG}} = \left(\sum_{k=n}^{N} R_k^0 \left(({}^k r_{11} + {}^k r_{12} + {}^k r_{13}) m_1 + ({}^k r_{21} + {}^k r_{22} + {}^k r_{23}) m_2 + {}^k p_{k+1-\mathrm{link}} m_p \right) \right) / m_{p-\mathrm{new}}, \quad (51)$$

where ${}^k r_{1i}, {}^k r_{2i}$ are the position vector of the mass center of cylinder and piston of the ith limb of the $(k+1)$th link in the kth reference frame respectively, and ${}^k p_{k+1-\mathrm{link}}$ is the position vector of upper platform of the $(k+1)$th link presented in the kth frame. In this formula, the mass of each element is multiplied by the position vector of that element in the kth frame. To revise the equation, a single term is added to the second row of Eq. (35) and the new mass and moment of inertia are replaced with the old ones,

$$F_p = \begin{bmatrix} f_p \\ n_p \end{bmatrix} = \begin{bmatrix} f_e + m_{p-\mathrm{new}} g - m_{p-\mathrm{new}} \dot{v}_p \\ n_e - {}^0 I_{p-\mathrm{new}} \dot{\omega}_p - \omega_p \times ({}^0 I_{p-\mathrm{new}} \omega_p) + r_{\mathrm{CG}} \times m_{p-\mathrm{new}} g \end{bmatrix}. \quad (52)$$

6. Simulation

6.1. Kinematic simulation

In this section, three types of desired trajectories for the center of upper platform are examined and the inverse kinematic results are presented. The desired trajectories are selected such that the system expresses its nonlinearity. The circular trajectory is defined as follows:

$$\begin{aligned} x_d &= R \sin(\omega t), \\ y_d &= R \cos(\omega t), \end{aligned} \quad (53)$$

where $R = 1$ cm and $\omega = \pi$ radians per second (Fig. 7(a)). The z-coordinate of upper platform is calculated automatically according to the constraint. The small radius of circular path is due to the limited workspace of mechanism. In kinematics simulation section, it is assumed that the manipulator has one link. The manipulator parameters used in simulation almost coincide with the fabricated manipulator shown in Fig. 1. The geometrical and inertial parameters are listed in Table I.

Assumption 1: There is no external load on the end-effector and the friction is negligible.

https://doi.org/10.1017/S0263574714002355 Published online by Cambridge University Press

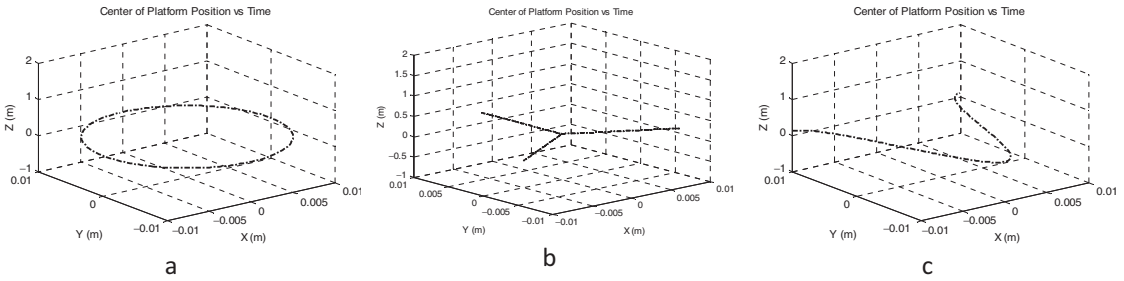

Fig. 7. The desired position of the center of upper platform in (a) circular trajectory for $R = 1$ cm, (b) star trajectory for $k = 5$, and (c) sinusoidal trajectory.

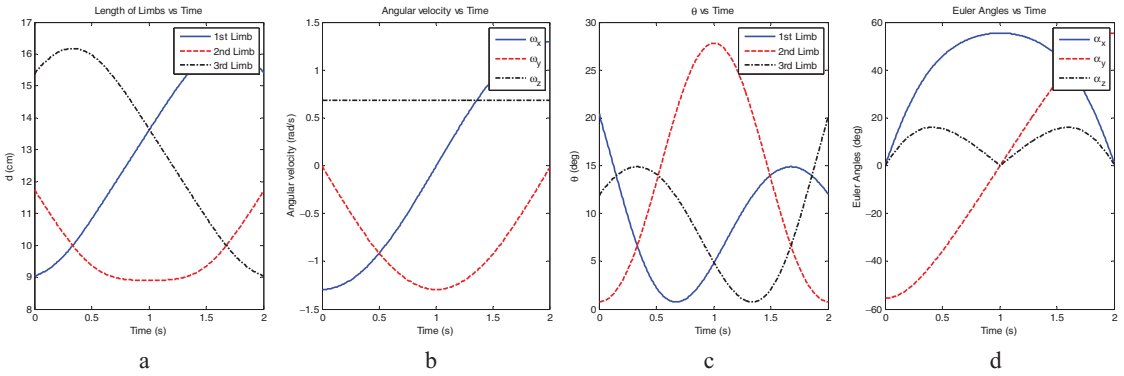

Fig. 8. (a) The length of limbs, (b) the angular velocity of upper platform, (c) the angle of each limb, and (d) the Euler angle in the circular trajectory of upper platform.

Figure 8 presents the inverse kinematic results in circular trajectory. The length of limbs, the angular velocity of upper platform, the angle of each limb (θ_i), and the Euler angle of upper platform are shown in this figure. First, it can be observed that the length of limbs vary around 12 cm, which is the length of each limb in the initial configuration of mechanism. Second, the sum of limb lengths is constant as stated in Eq. (1). It is worth mentioning that at the beginning of the motion, where $x_d = 0$ and $y_d = 1$ cm, d_1 is nearly equal to its natural length, d_2 and d_3 have taken the opposite direction to satisfy the constraint and make the upper platform move in the y-direction. It causes quite a large Euler angle in y as shown in Fig. 8(d). Since the initial position coincides with the direction of the second link, θ_2 is much smaller than θ_1 or θ_3 (Fig. 8(c)). The angular velocity of upper platform in x, y, and z-directions are obtained from the constraint Eq. (20). It can be observed that the z-component (yaw) of angular velocity is less than the other components since the circular trajectory did not require the yaw angular velocity.

Several ways have been adopted to check the correctness of results. For example, the numerical derivative of limb lengths must be equal to the $\dot{d}_i$ obtained in Eq. (21), and the y-coordinate of velocity and acceleration of b_i must be zero as stated in Eqs. (18) and (26). Equation (1), its derivative, and also its second derivative must be satisfied.

In order to validate the inverse kinematic results, a special trajectory named as star is defined in six stages as follows to simplify the interpretation of results:

$$[x_d \quad y_d]^T = \begin{cases} k[a_{1x}t_1 & a_{1y}t_1]^T & 0 \le t_1 \le 1 \\ k[-a_{1x}t_2 + a_{1x} & -a_{1y}t_2 + a_{1y}]^T & 0 \le t_2 \le 1 \\ k[a_{2x}t_3 & a_{2y}t_3]^T & 0 \le t_3 \le 1 \\ k[-a_{2x}t_4 + a_{2x} & -a_{2y}t_4 + a_{2y}]^T & 0 \le t_4 \le 1 \\ k[a_{3x}t_5 & a_{3y}t_5]^T & 0 \le t_5 \le 1 \\ k[-a_{4x}t_6 + a_{4x} & -a_{4y}t_6 + a_{4y}]^T & 0 \le t_6 \le 1, \end{cases} \tag{54}$$

https://doi.org/10.1017/S0263574714002355 Published online by Cambridge University Press

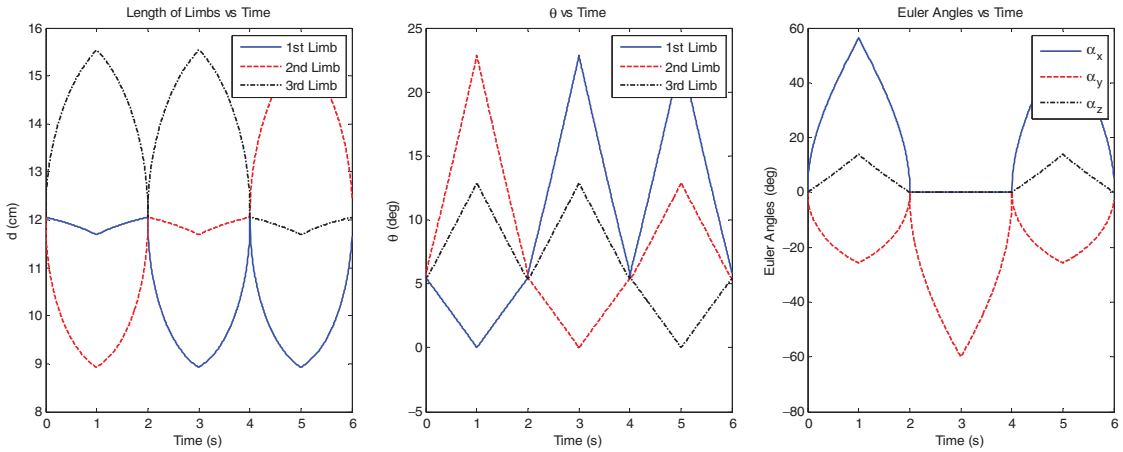

Fig. 9. (a) The length of limbs, (b) the angle of each limb, and (c) the Euler angle in the star trajectory of upper platform.

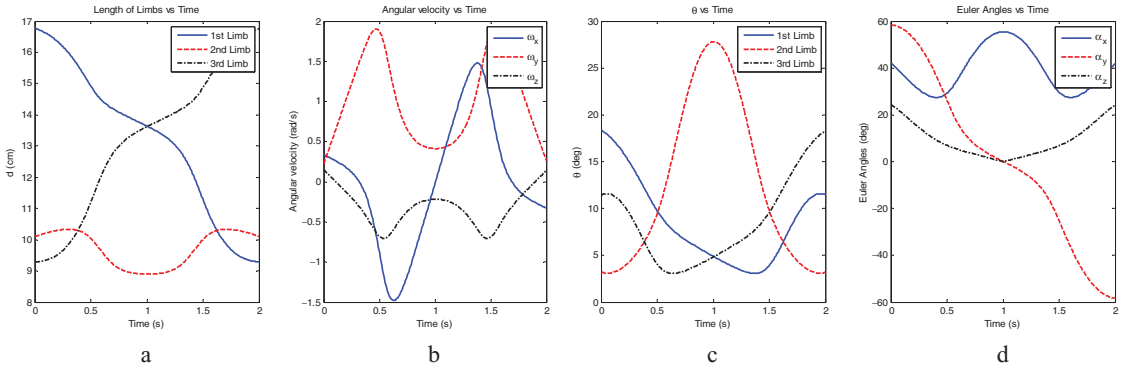

Fig. 10. (a) The length of limbs, (b) the angular velocity of upper platform, (c) the angle of each limb, (d) the Euler angle in the sinusoidal trajectory of upper platform.

where a is the position vector of lower platform whose length is 5.8 cm, and k is a scaling factor. The desired trajectory in which the size of star's arm is 1.2 cm is shown in Fig. 7(b). Each stage lasts for 1 s and the desired velocity is constant in each stage. The center of upper platform moves in the direction of the symmetric axis of triangle from the center position, and then it moves back to the center.

Figure 9 presents the inverse kinematic results of the star trajectory. It can be observed in Fig. 9(a) that when upper platform moves from the center toward a certain limb, the length of that limb does not vary as much as can be inferred qualitatively. Besides, angle θ_i of that limb decreases and tends to become vertical.

The third trajectory is a sinusoidal path in the x–y plane and is more complicated for this manipulator than previous trajectories, and defined as

$$\begin{aligned} x_d &= 0.01t - 0.01, \\ y_d &= -0.01\cos(100\pi x_d). \end{aligned} \tag{55}$$

The sinusoidal trajectory is shown in Fig. 7(c) and kinematic results are presented in Fig. 10. The sum of limb length is constant, and is equal to 0.362 m.

https://doi.org/10.1017/S0263574714002355 Published online by Cambridge University Press

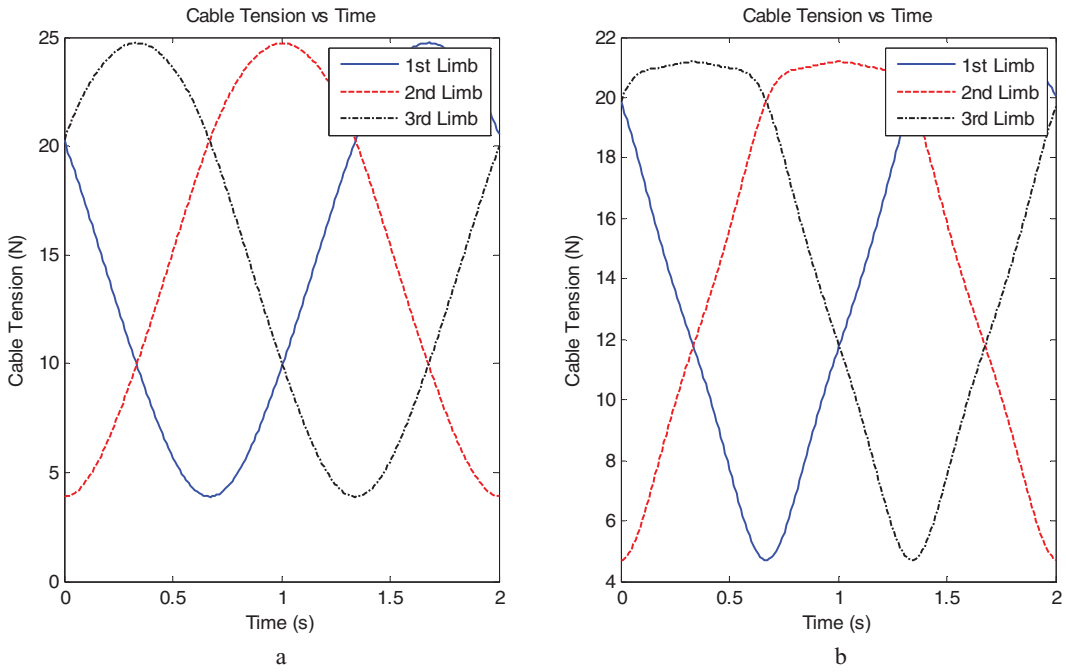

Fig. 11. Force of actuators (cable) in circular trajectory when (a) the lowest link is unlocked, and (b) the link on the top of the lowest link is unlocked.

6.2. Dynamics simulation

In this section, the manipulator is assumed to have four links. In each simulation, first the lowest link is unlocked and the remaining links are locked, and second, the link on the top of the lowest link is unlocked and the remaining links are locked to compare the cable tension.

Assumption 2: It is assumed that the manipulator is in the upright configuration and all upper platforms are horizontal at the beginning. The height of manipulator in this configuration is 0.48 m.

Since the workspace of the manipulator with four links is large enough, the circular trajectory defined in Eq. (53) is selected for $R = 15$ cm and $\omega = \pi$. Figure 11 shows cable tension for both stages of simulation. When the lowest link is unlocked, the range of motion of upper platform of that link is too small (4 mm) and the maximum Euler angle of upper platform is 25°. When the link on the top of the lowest link is unlocked, the range of motion becomes bigger (10 mm) and the maximum Euler angle is of 40°. Although the range of motion and acceleration is smaller in the first stage, the moving mass and moment of inertia of moving parts are bigger and cause larger cable tension. As shown in this figure, the maximum range of cable tension in the first and second stage is 20.84 N and 16.45 N respectively.

The star trajectory with arm's length of 11.6 cm is selected to increase the range of motion of upper platform.

Figure 12 shows cable tension for both stages of simulation. As shown in this figure, the maximum range of cable tension in the first and second stage is 11.27 N and 7.87 N respectively. It is worth mentioning that the tension of second and third cables in the interval of [0, 2] s is larger than the tension of the first cable since the upper platform is moving in the direction of the first limb and the opposite cables must be pulled. This fact is true for remaining part of the trajectory.

7. Conclusions

The kinematic and dynamic analysis of a N-3RPS manipulator with lockable joints is presented in this paper. In this manipulator all links have 3RPS mechanism, and are connected serially. In each link, a hydraulic locking mechanism is installed. The locking mechanism reduces the complexity of actuation system and decreases the weight of manipulator. Since the base mechanism of the manipulator is 3RPS, the inverse and forward dynamics of this mechanism is introduced at the first

https://doi.org/10.1017/S0263574714002355 Published online by Cambridge University Press

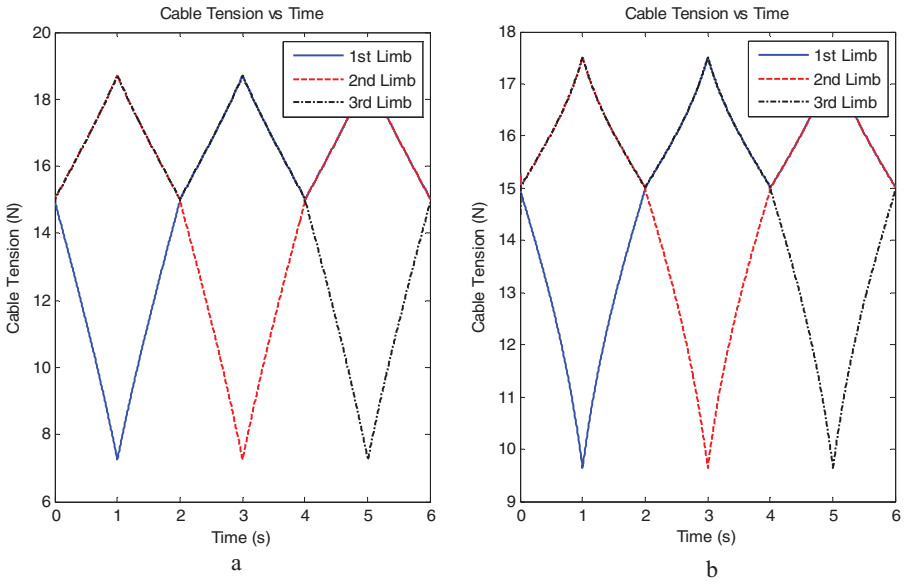

Fig. 12. Force of actuators in star trajectory when (a) the lowest link is unlocked, and (b) the link on the top of the lowest link is unlocked.

step. The dynamic analysis of the N-3RPS manipulator is presented in the next step. In the final step, several trajectories are given and the input forces of a 3-3RPS manipulator (with three links) are calculated. The simulations show the performance of analysis.

References

1. Y. Zhang, J. Wang and Y. Xia, "A dual neural network for redundancy resolution of kinematically redundant manipulators subject to joint limits and joint velocity limits," *IEEE Trans. Neural Netw. Learn. Syst.* **14**(3), 658–667 (2003).
2. H. Choset and W. Henning, "A follow the leader approach to serpentine robot motion planning," *J. Aerospace Eng.* **12**(2), 65–73 (1999).
3. K. J. Ning and F. Worgotter, "A novel concept for building a hyper-redundant chain robot," *IEEE Trans. Robot.* **25**(6), 1237–1248 (2009).
4. A. Meghdari, "Conceptual design and dynamics modeling of a cooperative dual-arm cam-lock manipulator," *Robotica* **14**(3), 301–310 (1996).
5. K. G. Osgouie, A. Meghdari and S. Sohrabpour, "Optimal configuration of dual-arm cam-lock robot based on task-space manipulability," *Robotica* **27**(1), 13–18 (2009).
6. B. Hu, Y. Lu, J. J. Yu and S. Zhuang, "Analyses of inverse kinematics, statics and workspace of a novel 3RPS-3SPR serial–parallel manipulator," *Open Mech. Eng. J.* **5**, 65–72 (2012).
7. J. Gallardo-Alvarado, C. R. Aguilar-Nájera, L. Casique-Rosas, J. M. Rico-Martínez and M. N. Islam, "Kinematics and dynamics of 2 (3-RPS) manipulators by means of screw theory and the principle of virtual work," *Mech. Mach. Theory* **43**(10), 1281–1294 (2008).
8. J. Gallardo, R. Lesso, J. M. Rico and G. Alici, "The kinematics of modular spatial hyper-redundant manipulators formed from RPS-type limbs," *Robot. Auton. Syst.* **59**(1), 12–21 (2011).
9. O. Ibrahim and W. Khalil, "Inverse and direct dynamic models of hybrid robots," *Mech. Mach. Theory* **45**(4), 627–640 (2010).
10. T. K. Tanev, "Kinematics of a hybrid (parallel–serial) robot manipulator," *Mech. Mach. Theory* **35**(9), 1183–1196 (2000).
11. M. Honarvar, "Design and Control of a New Tendon Actuated Manipulator With Lockable Joints," **In**: (Sharif University of Technology, 2008) pp. 14–42.
12. W. Khalil and O. Ibrahim, "General solution for the dynamic modeling of parallel robots," *J. Intell. Robot. Syst.* **49**(1), 19–37 (2007).
13. H. Pang and M. Shahinpoor, "Inverse dynamics of a parallel manipulator," *J. Robot. Syst.* **11**(8), 693–702 (1994).
14. L. W. Tsai, "Solving the inverse dynamics of a Stewart–Gough manipulator by the principle of virtual work," J. Mech. Des-T. (ASME) **122**(1), 3–9 (2000).
15. J. Angeles, *Fundamentals of Robotic Mechanical Systems: Theory, Methods, and Algorithms* (Springer, Berlin, Germany, 2006) pp. 287–363.

https://doi.org/10.1017/S0263574714002355 Published online by Cambridge University Press

16. J. Gallardo, J. Rico, A. Frisoli, D. Checcacci and M. Bergamasco, "Dynamics of parallel manipulators by means of screw theory," *Mech. Mach. Theory* **38**(11), 1113–1131 (2003).
17. T. Geike and J. McPhee, "Inverse dynamic analysis of parallel manipulators with full mobility," *Mech. Mach. Theory* **38**(6), 549–562 (2003).
18. J. J. Murray and G. H. Lovell, "Dynamic modeling of closed-chain robotic manipulators and implications for trajectory control," *IEEE Trans. Robot. Autom.* **5**(4), 522–528 (1989).
19. Y. J. Lin and S. M. Song, "A comparative study of inverse dynamics of manipulators with closed-chain geometry," *J. Robot. Syst*. **7**(4), 507–534 (1990).
20. S. Staicu, "Inverse Dynamics of the Spatial 3-RPS Parallel Robot," *Proc. Rom. Acad. A* **13**(1), 62–70 (2012).
21. Y. G. Li, H. T. Liu, X. M. Zhao, T. Huang and D. G. Chetwynd, "Design of a 3-DOF PKM module for large structural component machining," *Mech. Mach. Theory* **45**(6), 941–954 (2010).
22. S. Staicu, "Modèle dynamique en robotique," *UPB Sci. Bull. D* **61**(3–4), 5–19 (1999).
23. S. Staicu, "Methodes matricielles en cinématique des mécanismes," *UPB Sci. Bull. D* **62**(1), 3–10 (2000).
24. M. Shafahi, "Optimization, Manufacturing and Utilization of a New Tendon Actuated Hyper Redundant Manipulator," **In**: *Mechanical Engineering* (Sharif University of Technology, 2011) pp. 33–79.
25. A. Taherifar, A. Alasty, H. Salarieh and M. Boroushaki, "Path planning for a hyper-redundant manipulator with lockable joints using PSO," *Proceedings of the, 2013 First RSI/ISM International Conference on Robotics and Mechatronics (ICRoM)*, Tehran, Iran (2013) pp. 224–229.

https://doi.org/10.1017/S0263574714002355 Published online by Cambridge University Press